# Fuel reactivity controlled compression ignition (RCCI): a pathway to controlled high-efficiency clean combustion

**S L Kokjohn**[*]**, R M Hanson, D A Splitter,** and **R D Reitz**
Department of Mechanical Engineering, The University of Wisconsin–Madison, Madison, Wisconsin, USA

**Abstract:** A fuel reactivity controlled compression ignition (RCCI) concept is demonstrated as a promising method to achieve high efficiency – clean combustion. Engine experiments were performed in a heavy-duty test engine over a range of loads. Additionally, RCCI engine experiments were compared to conventional diesel engine experiments. Detailed computational fluid dynamics modelling was then used to explain the experimentally observed trends. Specifically, it was found that RCCI combustion is capable of operating over a wide range of engine loads with near zero levels of $NO_x$ and soot, acceptable pressure rise rate and ringing intensity, and very high indicated efficiency. For example, a peak gross indicated efficiency of 56 per cent was observed at 9.3 bar indicated mean effective pressure and 1300 rev/min. The comparison between RCCI and conventional diesel showed a reduction in $NO_x$ by three orders of magnitude, a reduction in soot by a factor of six, and an increase in gross indicated efficiency of 16.4 per cent (i.e. 7.9 per cent more of the fuel energy was converted to useful work). The simulation results showed that the improvement in fuel conversion efficiency was due both to reductions in heat transfer losses and improved control over the start- and end-of-combustion.

**Keywords:** engine performance, fuel efficiency, thermal efficiency, HCCI, PCCI, combustion, pollutant emissions reduction

## 1   INTRODUCTION

Rising fuel costs and a focus on reduction of greenhouse gases has driven the need for increased efficiency from the internal combustion engine. This need for increased efficiency has placed the diesel or CI engine (note that all acronyms are defined in the Appendix) in the spotlight due to its superior fuel efficiency compared to SI engines. However, under conventional diesel operation, regions of the combustion chamber pass through both rich and lean high-temperature regions, forming soot and $NO_x$, respectively. Soot can be effectively reduced through the use of a DPF; however, DPFs require periodic regeneration (i.e. removal of collected soot), which often increases fuel consumption. Additionally, since diesel engines generally operate lean of stoichiometric, UHC and CO are generally not available to reduce $NO_x$ to nitrogen using a TWC. Several attempts have been made to operate CI engines stoichiometric such that a TWC can be used for $NO_x$ reduction [1]; however, these efforts generally resulted in poor fuel economy; thus removing the CI engine's advantages over the SI engine. In addition to stoichiometric-TWC $NO_x$ reduction, forms of $NO_x$ after-treatment compatible with lean operation exist (i.e. LNT and SCR). An LNT is essentially a TWC reformulated to enhance storage of $NO_x$ during lean operation [2]. As such, LNTs provide $NO_x$ reduction in a very similar manner as a conventional TWC; that is, $NO_x$ is reduced to $N_2$ through reactions with products of

*Corresponding author: Department of Mechanical Engineering,*
*The University of Wisconsin–Madison, 1011 Engineering*
*Research Building 1500 Engineering Dr. Madison, WI 53711*
*USA*
*email: kokjohn@wisc.edu*

rich combustion (CO, HC, and $H_2$) [2]. An engine relying on an LNT for $NO_x$ reduction must periodically operate rich to reduce the stored $NO_x$; thus, fuel efficiency is reduced. In contrast to LNT technology, SCR technology can be used for $NO_x$ reduction without the need to operate rich; thus the fuel economy benefits of the lean-burn CI engine are retained. However, similar to the required periodic rich operation of LNT technology, SCR technology requires the introduction of a reducing agent (urea). The urea is stored on the vehicle and is injected into the exhaust system, providing no useful work; thus the consumed urea used for $NO_x$ reduction can be considered additional 'fuel' consumption.

Considering the presented discussion it is clear that to maximize overall engine efficiency, an engine should minimize the need for after-treatment-type emissions reduction. Accordingly, reduction of $NO_x$ and soot in-cylinder has been investigated by many researchers. Most of the current strategies can be lumped into the category of premixed LTC. Lower combustion temperatures result in $NO_x$ reduction due to the high activation energy of NO formation reactions [3]. In addition, utilizing long ignition delay times allows adequate time for mixing prior to the start of combustion; thus, rich regions are reduced and soot formation is inhibited. Many researchers have shown that HCCI and PCCI concepts are promising techniques for simultaneous $NO_x$ and soot reduction [4–10]. In addition to significant $NO_x$ and soot reductions, premixed LTC operation can provide fuel efficiency advantages due to reduced combustion duration and lower HT losses. In the past HCCI and PCCI combustion generally suffered from high levels of CO and UHC emissions; however, in recent years several researchers have demonstrated boosted HCCI and PCCI combustion featuring nearly 100 per cent combustion efficiency [7, 11, 12]. These improvements came through the use of piston designs featuring minimum crevice volumes as well as highly boosted operation.

Due to the existing fuel infrastructure, most HCCI and PCCI research has been conducted using either strictly gasoline or diesel fuel. However, in their neat forms, each fuel has specific advantages and shortcomings for PCI operation. Gasoline has a high volatility; thus, evaporation is rapid and a premixed charge can be obtained using PFI. Furthermore, Kalghatgi [13] and Kalghatgi et al. [14, 15] have shown promising emissions and performance results using a gasoline partially PCI strategy. In their work, gasoline's resistance to auto-ignition (i.e. low cetane number) was exploited to extend the pre-combustion mixing time in order to

achieve simultaneous reductions in $NO_x$ and soot emissions. However, other researchers (e.g. [16, 17]) have shown that the poor auto-ignition qualities of gasoline can make it difficult to achieve combustion at low-load conditions. Conversely, diesel fuel has superior auto-ignition qualities; however, this can result in difficulty controlling the combustion phasing as engine load is increased. Therefore, when neat diesel fuel is used in a PCI strategy, high levels of EGR are required to phase combustion appropriately [10].

Experiments performed by Bessonette et al. [18] have suggested that the best fuel for HCCI operation may have auto-ignition qualities between that of diesel fuel and gasoline. Using a compression ratio of 12:1 and a fuel with a derived cetane number of ~27 (i.e. a gasoline boiling range fuel with an octane number of 80.7), they were able to extend the HCCI operating range to 16 bar BMEP – a 60 per cent increase in the maximum achievable load compared to operation using traditional diesel fuel. Furthermore, their results showed that low-load operation, below 2 bar BMEP, required a derived cetane number of ~45 (i.e. traditional diesel fuel). Thus, it may be beneficial to explore HCCI operation using fuel blends optimized for specific operating conditions.

Inagaki et al. [19] investigated dual-fuel PCI operation as a means for reducing the EGR requirements of PCI strategies. Using premixed iso-octane and direct injected diesel fuel, they were able to operate in PCI mode at 12 bar IMEP. Furthermore, they showed that stratification of fuel reactivity (rather than only equivalence ratio) resulted in reduced rates of heat release and reasonable combustion noise.

Based on the work of Bessonette et al. [18] and Inagaki et al. [19], it is likely that different fuel blends will be required at different operating conditions (e.g. a high cetane fuel at light load and a low cetane fuel at high load). Thus, it is desirable to have the capability to operate with fuel blends covering the spectrum from neat gasoline to neat diesel fuel depending on the operating regime. This work proposes PFI of gasoline and early cycle DI of diesel fuel.

HCCI combustion is a kinetically controlled process; therefore, the combustion phasing is very sensitive to charge gas temperature. In the laboratory, where intake temperature and EGR can be precisely controlled, single-fuel HCCI combustion can demonstrate very promising results. However, in practice the charge gas temperature of practical engines depends on many factors and varies with speed, load, and operating environment. To understand the motivation for investigating in-cylinder fuel blending, Fig. 1 shows constant-volume ignition
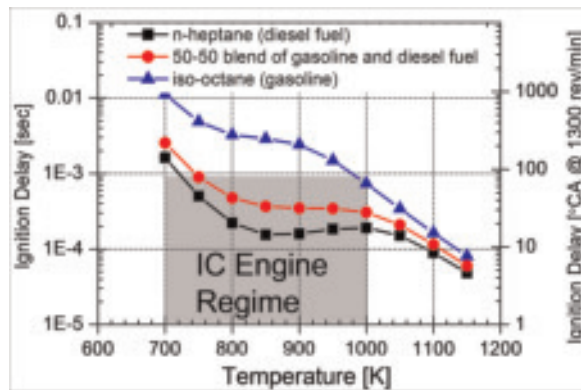
**Fig. 1** Constant-volume ignition delay times for neat n-heptane, neat iso-octane, and a 50-50 blend of iso-octane and n-heptane calculated using the SENKIN code [**44**] and a reduced PRF mechanism. This set of simulations was performed at an initial pressure of 70 bar and an equivalence ratio of 0.5. The shaded area shows representative TDC temperatures and ignition delay times representitive of conditions seen in internal combustion engines

**Table 1** Test engine geometry

| Base engine type | Caterpillar SCOTE |
|---|---|
| Bore × stroke | 13.72 × 16.51 cm |
| Connecting rod length | 26.16 cm |
| Squish height | 0.157 cm |
| Piston pin offset | None |
| Displacement | 2.44 L |
| Geometric compression ratio | 16.1:1 |
| Swirl ratio | 0.7 |
| Bowl type | Open crater |
| Number of valves | 4 |
| IVO | −335° ATDC |
| IVC | −85 and −143° ATDC |
| EVO | 130° ATDC |
| EVC | −355° ATDC |

delay calculations using a PRF mechanism developed by Ra and Reitz [**20**] for neat iso-octane, neat n-heptane, and a 50-50 blend of iso-octane and n-heptane. For optimum thermal efficiency, the combustion phasing must be precisely controlled and to maintain high efficiency an engine must be able to accommodate changes in the operating conditions (e.g. charge temperature) while maintaining the optimum combustion phasing. Figure 1 shows that, since each fuel has a unique ignition delay–temperature curve, each fuel will be limited to a narrow operating range where peak efficiency can be achieved. For example, if a representative temperature of 750 K is selected and the ignition delay that is required to achieve the optimum combustion phasing is ~40° CA, neat diesel fuel would provide the optimum fuel reactivity to achieve peak efficiency. However, if the operating conditions changed such that the representative temperature increased to 800 K, neat diesel fuel would result in overly advanced combustion phasing, increased HT losses, and reduced thermal efficiency. However, by using in-cylinder fuel blending, peak efficiency could be maintained by moving from neat diesel fuel to a 50-50 blend of diesel and gasoline.

## 2 EXPERIMENTAL SETUP

A single cylinder, HD diesel engine based on a Caterpillar 3401 SCOTE was used for all engine experiments in this study. The engine specifications are shown in Table 1 and a schematic of the laboratory setup is shown in Fig. 2. This engine is a typical HD-type diesel engine with a geometric compression ratio of 16.1:1, an open crater piston, and a low swirl head. Notice that two different cam shafts were used for this work. The stock camshaft of the HD test engine has an IVC timing of −143° ATDC. However, to aid in combustion phasing control a modified camshaft with an IVC timing of −85° ATDC was used. Both cams have the same IVO timing of −335° ATDC.

In this work, a premixed charge of gasoline is achieved using an automotive type PFI system and the diesel fuel is delivered using a common rail type DI system. The specifications for the port-fuel-injector and direct-injector are given in Table 2 and Table 3, respectively.

Cylinder pressure was measured with a Kistler model 6043 Asp water-cooled pressure transducer in conjunction with a Kistler model 510 charge amplifier. Acquired cylinder pressure traces were averaged for 500 cycles. Intake air flow was measured using choked flow orifices. To obtain choked flow for a variety of engine operating conditions, combinations of six different sized orifices were used to gain the desired intake air flowrate. Intake air was heated with two immersion-style heaters and PID control to ±1 °C. Both the intake and exhaust system surge tank pressures were equipped with PID control to ±0.7 kPa. PM measurements were performed with an AVL model 415s smoke meter. PM measurements of FSN, mass per volume (mg/m$^3$), and specific emissions (g/kW-h) were related with the factory AVL calibration and averaged between five samples of a 2 L volume each with paper-saving mode off. All gaseous emissions measurements were performed with a five gas emissions bench. The EGR rate was determined through the ratio of intake $CO_2$ to exhaust $CO_2$ levels.
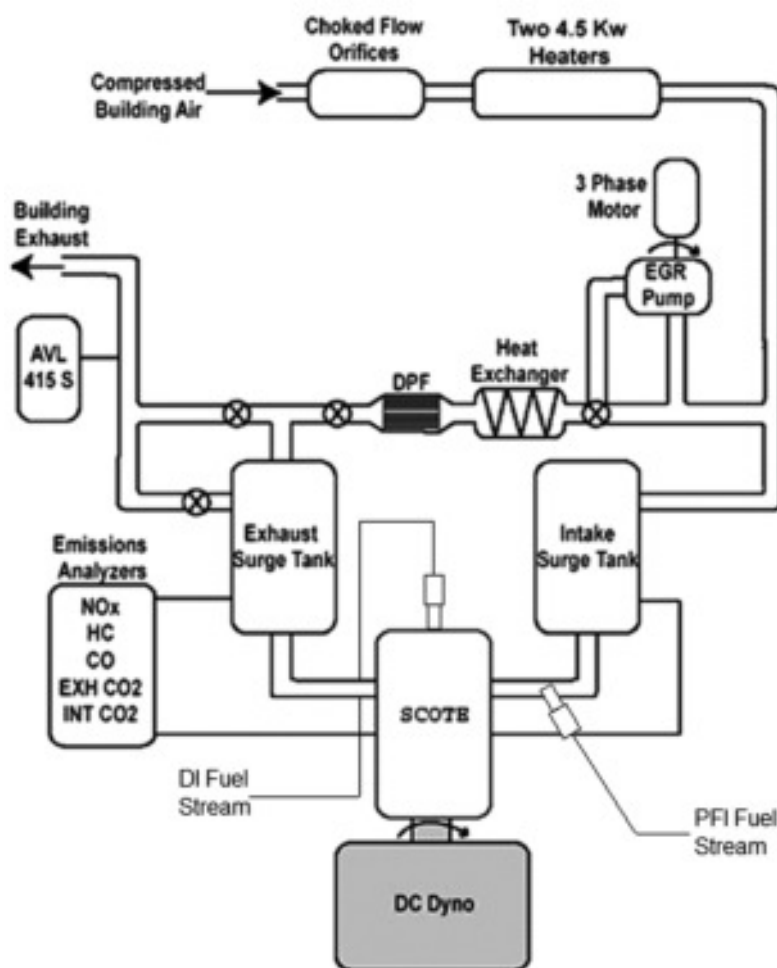
**Fig. 2** Diagram of the engine laboratory setup. The premixed fuel is delivered through the PFI of Table 2 and the direct-injected fuel is delivered through a common rail fuel injected as specified in Table 3.

**Table 2** Port fuel injector specifications

| | |
|---|---|
| Steady flow rate at 3 bar | 12.5 cc/s |
| Included spray angle | 15° |
| Fuel pressure | 5.17 bar |

Gaseous emissions were averaged for 30 s after attaining steady state operation.

The EGR system consists of an electrically driven supercharger and a diesel particulate filter to prevent fouling of the EGR cooler and supercharger. The EGR supercharger was implemented as a pump to maintain constant EGR levels with constant surge tank pressures as the DPF fills.

Commercially available 91.6 antiknock index ((R + M)/2) gasoline and ultra-low sulfur diesel fuel with a cetane number of 46 was used for all tests. Table 4 and Table 5 show an independent lab analysis of the fuel properties.

## 3 COMPUTATIONAL MODEL

Computations were performed using the KIVA-3v release 2 coding [21] with improvements to many physical and chemistry models developed at the ERC [22–25]. The KIVA-3v code is coupled with the CHEMKIN II solver for detailed chemistry calculations. In this study the chemistry of gasoline and diesel fuel are represented by that of iso-octane and n-heptane, respectively. A reduced reaction mechanism made up of 45 species and 142 reactions [20] describes the combined oxidation of n-heptane and iso-octane. Note that many studies (e.g. Ra and Reitz [26]) have shown that the combustion characteristics of gasoline and diesel are closely represented by iso-octane (i.e. PRF 100) and n-heptane (i.e. PRF 0), respectively. This approach has also been shown to yield acceptable agreement for blends of gasoline and diesel fuel (e.g. Kokjohn *et al.* [6], Hanson *et al.* [27], and Splitter *et al.* [28]).

**Table 3** Common rail injector specifications

| | |
|---|---|
| Number of holes | 6 |
| Steady flow rate at 100 bar | 33.3 cc/s |
| Hole diameter | 250 μm |
| Included spray angle | 145° |
| Injection pressure | 400 to 800 bar |

**Table 4** Gasoline fuel properties

| Distillation curve method | ASTM D86 |
|---|---|
| Initial boiling point | 38.9 °C |
| Temperature 10 per cent evaporated | 69.4 °C |
| Temperature 50 per cent evaporated | 105.0 °C |
| Temperature 90 per cent evaporated | 160.6 °C |
| Final boiling point | 215.6 °C |
| LHV | 43.2 MJ/kg |
| MON | 87.8 |
| RON | 95.6 |
| (R + M)/2 | 91.6 |
| Ethanol | 0% |
| H/C ratio | 1.88 |
| Density | 756 kg/m$^3$ |

**Table 5** Diesel fuel properties

| | |
|---|---|
| Viscosity (at 40 °C) | 2.71 cSt |
| Surface tension (at 25 °C) | 30.0 dyne/cm |
| LHV | 42.5 MJ/kg |
| Cetane number | 46.1 |
| H/C ratio | 1.74 |
| Density | 856 kg/m$^3$ |

The physical properties (for spray and mixing processes) of diesel fuel are represented by tetradecane. Of course, the multi-component vaporization of the diesel fuel used in the experiments is not captured by this approach (i.e. the distillation curve of diesel fuel is not reproduced). It is possible that the differences between single- and multi-component vaporization result in differences in the fuel distribution prior to and during combustion. PCCI combustion has been shown to be very sensitive to the mixture preparation details (e.g. Opat et al. [10]); therefore, the simplified vaporization model should be borne in mind when accessing the observed differences between the simulations and experiments. However, this approach has been used in numerous studies and has been shown to yield acceptable results. For example, Shuai et al. [29] compared model predicted fuel distributions to fuel distributions acquired using planar laser-induced fluorescence in an optically accessible engine operating in a low-temperature combustion mode. They showed that, under low-temperature combustion conditions, the spray models used in the current study accurately reproduced the measured fuel distribution.

Soot is predicted using a phenomenological soot model [25] based on the approach of Hiroyasu and Kadota [30]. The soot model used in the present study uses acetylene as an inception species, which allows the soot model to be coupled to the chemistry solver through the addition of 13 reactions involving acetylene. $NO_x$ emissions are predicted using a reduced NO mechanism [31] consisting of four additional species and 12 reactions.

The spray model employed in this study uses the LDEF approach. In order to reduce the grid size dependency of the LDEF spray model and allow accurate spray simulation on a relatively coarse grid, the Gasjet model of Abani et al. [23] is used to model the relative velocity between the droplets and gas phase in the near nozzle region. Their approach assumes that the relative velocity between a droplet and the gas phase is equal to that between the droplet and a turbulent gas-jet with the same mass and momentum of that of the injected fuel.

Droplet breakup is modelled using the hybrid KH – RT model described by Beale and Reitz [22]. The droplet collision model is based on O'Rourke's model; however, a radius of influence method is used to determine the possible collision partners to further reduce mesh dependency [32]. In addition, the collision model was expanded by Munnannur [32] to include a more comprehensive range of collision outcomes. The current implementation of the droplet collision model considers the effects of bounce, coalescence, and fragmenting and non-fragmenting separations. Droplet interactions with the wall are considered through a wall film submodel [33, 34], which includes the effects associated with splash, film spreading, and motion due to inertia.

Simulations were performed using the three-dimensional computational grid shown in Fig. 3. To reduce the computational burden, a 60° sector mesh (corresponding to a single nozzle hole of the six hole injector of this study) with periodic boundaries was used. Notice that the region above the top piston ring is resolved in this study; however, ring motion and flow past the compression rings are not included.

## 4 SCOPE AND OBJECTIVES

In the authors' previous studies [6, 27, 28, 35] RCCI combustion was explored through parametric studies at a fixed load. In this work, RCCI combustion is investigated over a range of engine loads from 4.6 to 14.6 bar gross IMEP. First, the experimental results are presented and emissions and
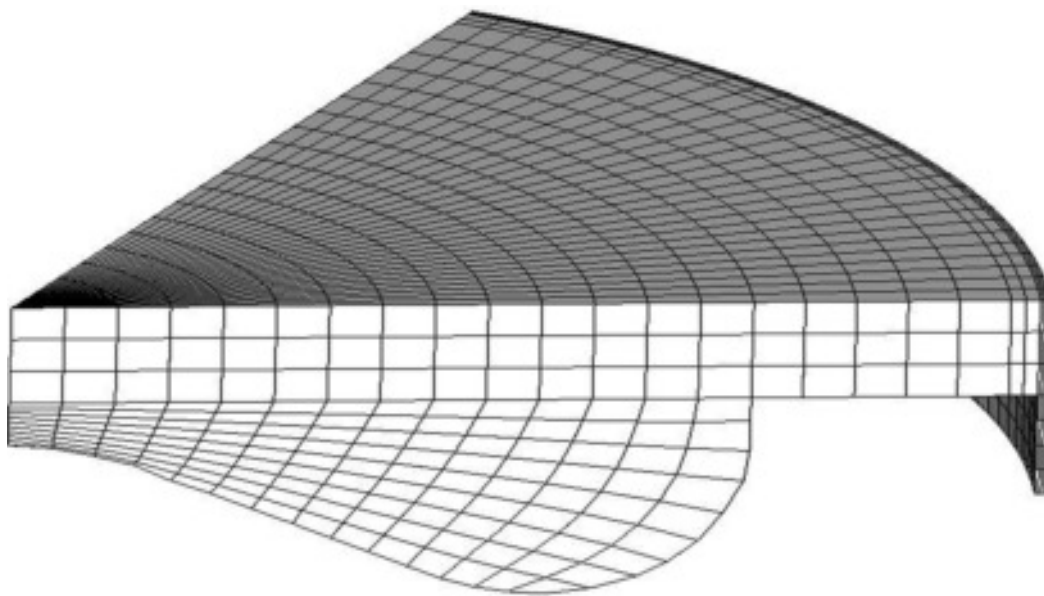
**Fig. 3** Computational grid with crevice volume. The grid consists of ~10 000 cells at BDC

performance are analysed. Next, operation at 9 bar IMEP is selected for further analysis using engine experiments and detailed CFD modelling. An experimental and numerical comparison between RCCI combustion and conventional diesel combustion operating at very similar conditions is presented. The effects of HT and the energy release characteristics are isolated by making comparisons with adiabatic operation.

## 5 INJECTION STRATEGY

To control the overall fuel reactivity and therefore combustion phasing, RCCI combustion uses in-cylinder blending of two fuels with differing auto-ignition characteristics. In this work, gasoline is delivered using the port-fuel-injector of Table 2 and diesel fuel is delivered using the common rail type direct-injector of Table 3. In addition to controlling the overall fuel-reactivity, in-cylinder fuel blending allows the generation of fuel reactivity gradients which result in control over the combustion duration.

In previous work RCCI operation was demonstrated at 6, 9, and 11 bar IMEP [27, 35] using an injection and in-cylinder fuel blending strategy developed with detailed CFD modelling [36]. The injection strategy is highlighted in Fig. 4. A first injection, shown in Fig. 4 as the squish conditioning pulse, is delivered near 60° BTDC targeting the squish region of the combustion chamber. The purpose of this injection is to control the fuel reactivity in the squish region ensuring complete combustion of the premixed gasoline in the outer portion of the combustion chamber. The second injection occurs near 35° BTDC and targets the bowl region of the combustion chamber. This injection event generates a relatively high reactivity region which acts as an ignition source.

## 6 RESULTS AND DISCUSSION

### 6.1 Engine performance over a range of loads

In this section RCCI combustion is demonstrated over a range of loads from 4.6 to 14.6 bar IMEP. The results presented here are a combination of the highest efficiency cases from a number of different experiments; thus, the engine parameters and operating variables are not fixed over the load sweep. Further note that to accommodate concurrent research projects at the ERC, the 4.6 bar IMEP case uses a slightly modified piston from that shown in Table 1 with a compression ratio of 15.5:1. This slight change in compression ratio is not expected to significantly influence the results. Table 6 shows the operating conditions over the range of loads considered in this work. Notice that the per cent gasoline was adjusted over the load sweep to maintain acceptable RI. In the present study, the gasoline percentage and EGR combinations were selected based on chemical kinetics simulations presented in the authors' previous work, see Kokjohn *et al.* [6]. In that work it was found that combustion should be phased later in the cycle as load is increased to control the RI (rate of pressure
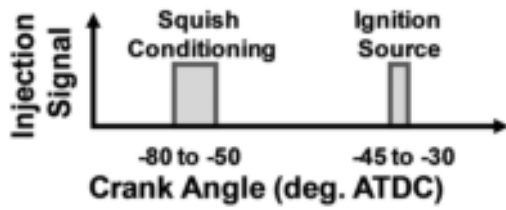
**Fig. 4** Injection strategy used for split injection dual-fuel RCCI combustion

rise). However, it should be noted that the results presented here have not been rigorously optimized and it is expected that different combinations of injection parameters, EGR levels, and gasoline percentages may yield similar results.

Figure 5 shows the measured and predicted cylinder pressures and AHRR over the load sweep. It can be seen that the simulations are able to accurately capture the combustion characteristics over the range of loads considered in this work. Figure 6 shows the measured and predicted emissions and performance over the range of loads. In Fig. 6 $NO_x$ and soot are shown on a gross indicated basis. The gross indicated efficiency is defined as the (gross-indicated-work)/(fuel energy). Because the engine operates under boosted condition for all but the lightest load, the PRR is not representative of knock [11]; therefore, the RI correlation of Eng [37] is used

$$RI = \frac{1}{2\gamma} \frac{[(dP/dt)_{\max}]}{P_{\max}} \sqrt{\gamma R T_{\max}} \qquad (1)$$

where $\gamma$ is the ratio of specific heats, $(dP/dt)_{\max}$ is the peak PRR, $P_{\max}$ is the peak pressure, $R$ is the ideal gas constant, and $T_{\max}$ is the peak temperature. In a similar engine, Dec and Yang [11] stated that RIs below 5 MW/m$^2$ resulted in acceptable combustion noise and knock-free operation; thus, in this work 5 MW/m$^2$ is used as an upper limit for acceptable combustion noise. Also shown in Fig. 6 are the US 2010 EPA HD on-highway truck limits for $NO_x$ and soot emissions (i.e. 0.268 g/kW-h and 0.0134 g/kW-h for $NO_x$ and soot, respectively).

Notice that the measured $NO_x$ is near zero and significantly below the 2010 EPA HD limits. Furthermore, it can be seen that soot is extremely low and below the 2010 EPA HD limits for all but the 6 bar IMEP point, which is very near the limit. It is possible that slight modifications to the operating parameters could be explored that would result in passing soot over the load sweep; however, since fuel efficiency is the focus of this study, methods for further soot reduction were not investigated.

Even with the current soot levels, it can be seen that dual-fuel RCCI combustion is a promising technique to meet the stringent emissions regulations without the need for $NO_x$ after-treatment and since soot is extremely low, if a DPF were required, the time between regenerations could be significantly extended compared to higher sooting operation.

Of more interest for this study are the fuel efficiencies and RIs. It can be seen that the gross indicated efficiency is ~49 per cent at the low-load condition, peaks at ~56 per cent at 9.3 bar IMEP, and levels out near 52 per cent for the higher loads. It should be noted that the most optimization has been conducted at the 9.3 bar IMEP operating point, which is likely the primary reason for the peak in the fuel efficiency at this point. However, it is still informative to investigate the fuel efficiency trends over the load sweep. Figure 7 shows the energy balances for each case. As previously stated, the gross indicated efficiency is calculated as the (gross work)/(fuel energy). The combustion losses are calculated as

$$\eta_{\substack{\text{comb.} \\ \text{loss}}} = \frac{\dot{m}_{\text{co}} LHV_{\text{co}} + \dot{m}_{\text{UHC}} LHV_{\text{fuel}}}{\dot{m}_{\text{fuel}} LHV_{\text{fuel}}} \qquad (2)$$

where $\dot{m}_{\text{co}}$ and $\dot{m}_{\text{UHC}}$ are the measured exhaust mass flowrates of CO and UHC, respectively, and $\dot{m}_{\text{fuel}}$ is the mass flowrate of the fuel. $LHV_{\text{CO}}$ and $LHV_{\text{fuel}}$ are the LHVs of the CO and fuel, respectively. Here it is assumed that the UHCs have the same heating value as the fuel. The exhaust energy is calculated from the measured exhaust temperature as

$$\eta_{\text{exhaust}} = \frac{\dot{m}_{\text{exh}}[h_{\text{exh}}(T_{\text{exh}}) - h_{\text{int}}(T_{\text{int}})]}{\dot{m}_{\text{fuel}} LHV_{\text{fuel}}} \qquad (3)$$

where $\dot{m}_{\text{exh}}$ is the mass flowrate of the exhaust, $h_{\text{exh}}$ and $h_{\text{int}}$ are the exhaust and intake enthalpies evaluated using the NASA database [38] assuming the exhaust contains only $O_2$, $N_2$, $CO_2$, $H_2O$, CO, UHC, and NO. Note that since all species except UHC were measured on a dry basis; thus, the water concentration in the exhaust stream was obtained using atom balancing. The heat loss contains the contributions of losses to the coolant, oil, and ambient and was obtained using an energy balance with the EGR loop located outside of the control volume; thus, the exhaust energy contribution contains heat rejected in the EGR heat exchanger.

Starting with the peak efficiency point (i.e. 9.3 bar IMEP), it can be seen that as the load is decreased, the HT and combustion losses increase;

**Table 6** Operating conditions for dual-fuel RCCI load sweep from 4.6 to 14.6 bar IMEP

|  | IMEP gross (bar) | | | | |
|---|---|---|---|---|---|
|  | 4.6 | 5.9 | 9.3 | 11.6 | 14.6 |
| Engine speed (rev/min) | 1300 | 1300 | 1300 | 1300 | 1300 |
| Fuel flowrate (g/s) | 0.57 | 0.71 | 1.02 | 1.36 | 1.74 |
| Per cent gasoline (% by mass) | 48 | 69 | 89 | 85 | 90 |
| Air flowrate (kg/s) | 0.026 | 0.029 | 0.03 | 0.026 | 0.026 |
| DI SOI 1 (°ATDC) | –62 | –63 | –58 | –67 | –58 |
| DI SOI 2 (°ATDC) | –37 | –34 | –37 | –36 | –37 |
| DI duration 1 (CA°) | 9.4 | 2.7 | 3.9 | 5.1 | 2.5 |
| DI duration 2 (CA°) | 5.1 | 5.9 | 2 | 2.3 | 4.3 |
| Per cent of DI fuel in pulse 1 (% by mass) | 65 | 32 | 67 | 68 | 37 |
| DI injection pressure (bar) | 400 | 600 | 800 | 800 | 800 |
| Intake surge tank pressure (bar) | 1.03 | 1.38 | 1.74 | 2 | 2.34 |
| Exhaust surge tank pressure (bar) | 1.1 | 1.45 | 1.84 | 2.13 | 2.52 |
| Intake surge tank temperature (°C) | 32 | 36 | 32 | 32 | 32 |
| Air : fuel ratio (–) | 45.4 | 40.9 | 29 | 19.1 | 15.1 |
| EGR rate (%) | 0 | 17 | 41 | 46 | 57 |
| Fuel MEP (bar) | 9.2 | 11.6 | 16.6 | 22.2 | 28.3 |
| IVC (°ATDC) | –85 | –85 | –143 | –85 | –85 |
| EVO (°ATDC) | 130 | 130 | 130 | 130 | 130 |
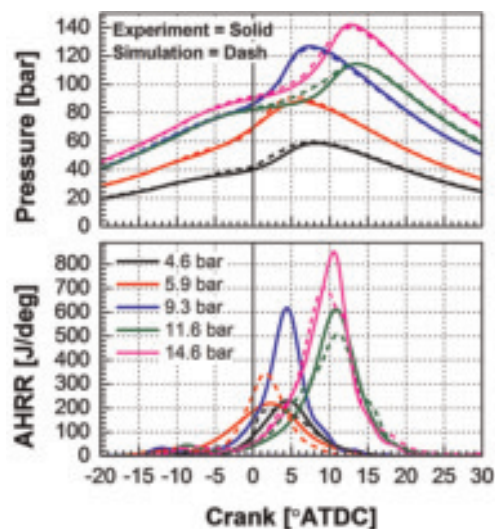


**Fig. 5** Comparison of cylinder pressure and AHRR over the load range from 4.6 to 14.6 bar IMEP. The experimental pressure and AHRR traces are shown in solid lines and the simulation results are shown in the dashed curves

a reasonable job capturing the emissions and engine performance over the load sweep. Notice that, at the 4.6 bar IMEP condition $NO_x$ is over-predicted by the model, but for the remainder of the load sweep $NO_x$ is predicted reasonably well. It should also be noted that for these cases both the measured and predicted $NO_x$ levels are very low; thus slight differences are not of significant concern. Comparing the measured and predicted soot emissions it can be seen that the models do a reasonable job capturing the soot trends; however, soot is significantly over-predicted at the 14.6 bar IMEP operating point. It should be noted that the soot model constants were held fixed over the load sweep (i.e. no attempts were made to 'tune' the soot model to each specific operating condition). Recall that the 14.6 bar IMEP operation point is near stoichiometric and some portions of the combustion chamber undergo slightly rich combustion. The over-prediction of soot as rich combustion is encountered may suggest that different soot model constants are required for rich and lean combustion. However, since the primary focus of this work is fuel consumption, adjustments to the soot model parameters were not explored. More importantly in the scope of this work, it can be seen that both the trends and magnitudes of the gross indicated efficiencies are closely captured by the models. Furthermore, because PRR and combustion noise are a major limiting factor for premixed operation, it is important to note that the simulations do an excellent job capturing both the trends and magnitudes of the RI.

Because the simulations reproduce the experimental results well and it appears that combustion
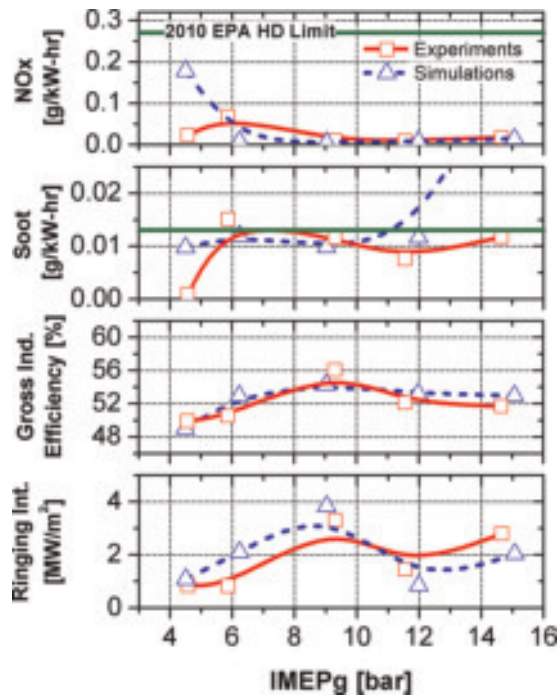
however, the exhaust losses decrease, nearly cancelling out the increase in HT losses. Thus, it can be seen that the main cause of the reduced efficiency at the lightest loads is the reduced combustion efficiency. Furthermore, as the load is increased past the peak efficiency point, the engine begins to approach stoichiometric operation; and thus it appears that the slight reduction in fuel consumption is also due to increased combustion losses.

Comparing the model predicted and measured values in Fig. 6 it can be seen that, similar to the combustion characteristics, the models do

**Fig. 6** Emissions and performance of dual-fuel RCCI over a range of loads from 4.6 to 14.6 bar IMEP. The solid horizontal lines show the US 2010 EPA on-highway truck emissions limits for $NO_x$ and soot
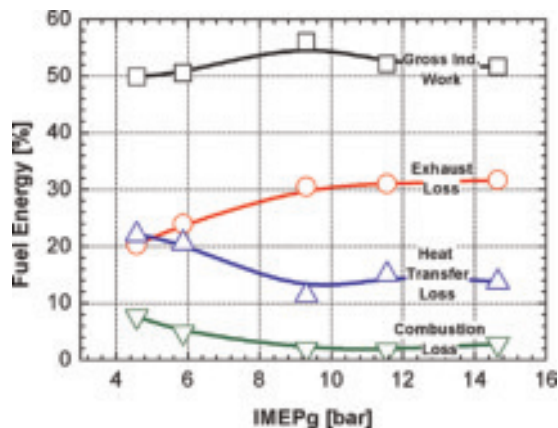


**Fig. 7** Flow of fuel energy over the load sweep

efficiency dominates the gross indicated efficiency trend, the simulations are used to understand the combustion efficiency trends observed in Fig. 7. Figure 8 shows iso-volumes of UHC and CO for the 4.6, 9.3, and 14.6 bar IMEP cases at a CA of 40° ATDC. It can be seen that at the light-load condition UHC is found in both the centreline and crevice regions. For this case CO is primarily found in the centreline region. The centreline UHC and CO is due to an overly lean region which does not release enough energy to completely oxidize the CO

and UHC. Moving to the 9.3 bar IMEP case it can be seen that UHC is only located in the crevice region and CO is only located in the region near the cylinder liner. The UHC in the crevice region is primarily unreacted iso-octane (gasoline) resulting from the premixed charge. The CO in the near liner region is due to relatively low temperatures due to HT from the gas to the cylinder liner. Additionally, as the crevice region outgasses late in the cycle, some UHC is converted to CO; however, temperatures fall rapidly and the CO in this region is not oxidized to $CO_2$. Finally, moving to the 14.6 bar IMEP case it can be seen that, similar to the 9.3 bar IMEP case, UHC is found only in the crevice region. However, in this case it can be seen that CO is present both in the near-liner region and the centreline. Similar to the 9.3 bar IMEP case, the CO near the liner is likely due to a combination of crevice outgassing and HT from the fluid resulting in low reaction rates. In this case, the centreline CO is not the result of overly lean regions, but rather locally rich regions created by the DI event. Recall that for this case operation occurs only slightly lean of stoichiometric (equivalence ratio of ~0.97), thus due to the DI event, some regions of the combustion chamber undergo rich combustion and insufficient oxygen is available to completely oxidize the CO.

Considering Fig. 8 the trend in combustion efficiency and gross indicated efficiency is clear. At the lightest loads operation borders on the lean limit for the premixed gasoline and complete oxidation of UHC and CO is difficult. At higher engine loads, as stoichiometric operation is approached, the DI event must be carefully controlled to avoid rich regions and incomplete combustion due to insufficient oxygen. Note that it is likely that at the highest engine loads the UHC and CO emissions could be reduced by increasing the boost pressure to eliminate the regions undergoing rich combustion. However, this has not been explored at this time. Finally, the peak in gross indicated efficiency and combustion efficiency at 9.3 bar IMEP is the result of operation avoiding both the lean and rich oxidation limits.

## 6.2 Comparison of conventional diesel and RCCI combustion

Previous studies [27] have suggested that dual-fuel RCCI shows increased gross indicated efficiency compared to conventional diesel operation through reduced HT losses and improved combustion phasing and duration. However, in the previous works direct comparisons were not made between conventional diesel and RCCI operation. In this section
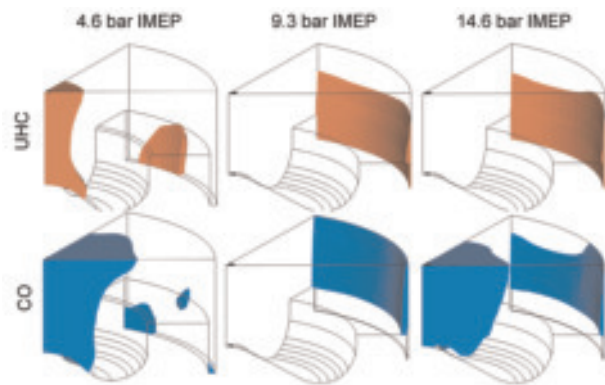
**Fig. 8** Iso-volumes showing regions with mass fractions of UHC (top) and CO (bottom) greater than 4000 ppm

**Table 7** Operating conditions for the comparison between conventional diesel and RCCI combustion

|  | RCCI | Conventional diesel |
|---|---|---|
| IMEP gross (bar) | 9.3 | 9.9 |
| Engine speed (rev/min) | 1300 | 1208 |
| Fuel flowrate (g/s) | 1.02 | 1.19 |
| Per cent gasoline (% by mass) | 89 | 0 |
| Air flowrate (kg/s) | 0.03 | 0.042 |
| DI SOI 1 (°ATDC) | −58 | −10 |
| DI SOI 2 (°ATDC) | −37 | NA |
| DI duration 1 (CA°) | 3.9 | 22 |
| DI duration 2 (CA°) | 1.95 | NA |
| Per cent of DI fuel in pulse 1 (% by mass) | 67 | 1 |
| DI injection pressure (bar) | 800 | 755 |
| Intake surge tank pressure (bar) | 1.74 | 1.72 |
| Exhaust surge tank pressure (bar) | 1.84 | 1.83 |
| Intake surge tank temperature (°C) | 32 | 36 |
| Air : fuel ratio (–) | 29 | 36 |
| EGR rate (%) | 41 | 0 |
| Fuel MEP (bar) | 16.6 | 20.5 |
| IVC (°ATDC) | −143 | −143 |
| EVO (°ATDC) | 130 | 130 |

direct comparisons are made between conventional diesel operation and RCCI operation at the 9 bar IMEP operating point. The conventional diesel case was taken from the experiments of Tess and Reitz [39] where conventional diesel operation was investigated at nearly identical conditions to those of the 9.3 bar IMEP case discussed in the previous section. Table 7 shows the operating conditions for the two cases. Note that the conventional diesel case was part of a size-scaling study [39] which required operation at a slightly lower speed than the RCCI cases investigated in this work. However, since the speeds differ by less than 100 rev/min it is thought that this will not influence the findings of this study.

The RCCI case is the 9.3 bar IMEP operating point from Table 6 operating using 89 per cent premixed gasoline and a split DI of diesel fuel. The first DI pulse occurs at −58° ATDC and the second pulse occurs at −37° ATDC. In this case 67 per cent of the direct-injected diesel fuel is delivered in the first DI pulse and the injection pressure is 800 bar. The RCCI case uses 41 per cent EGR providing an intake oxygen concentration of 15.8 per cent by volume. The conventional diesel case features a single DI occurring at −10° ATDC with an injection pressure of 755 bar. The conventional diesel case operates without EGR and for both cases the intake pressure is near 1.7 bar. Figure 9 shows a comparison of the measured and predicted cylinder pressure and AHRR for conventional and RCCI combustion. First of all, it can be seen that the models used in this study are capable of capturing the combustion characteristics over a wide range of operating conditions from the low-temperature combustion dual-fuel RCCI mode to the high-temperature, mixing-controlled conventional diesel mode. Table 8 shows the comparison of the measured and

predicted emissions and performance for these cases. Note that the exhaust temperature was not measured in the conventional diesel experiments of Tess and Reitz [39]; thus, the HT cannot be evaluated from the experimental results. However, given difficulties associated with accurately measuring the exhaust temperature (e.g. accounting for radiation from the thermocouple to the exhaust surge tank walls [40]) the model-predicted HT values likely provide more insight into the combustion process. For the model predictions, the HT considers only the closed portion of the cycle (i.e. from IVC to EVO). This is likely a reasonable approximation since a majority of the HT occurs during the energy release period near TDC. Since the simulations only consider the closed portion of the cycle, the temperature at EVO is not representative of the exhaust temperature; therefore, the exhaust energy is solved for using an energy balance. These approximations should be considered when comparing the relative quantities of HT and exhaust energy to other data; however, in this section the comparisons of the energy balances will rely completely on the model predictions and are therefore deemed acceptable.

Compared to conventional diesel combustion, RCCI demonstrates three orders of magnitude lower $NO_x$, a factor of six lower soot levels, and 16.4 per cent higher gross indicated efficiency (i.e. the RCCI case converts 7.9 per cent more of the fuel energy to useful work). However, RCCI combustion shows increased PRR, RI, and combustion losses (i.e. increased UHC and CO). However, it can be seen that the RI is well below the value of 5 MW/m$^2$
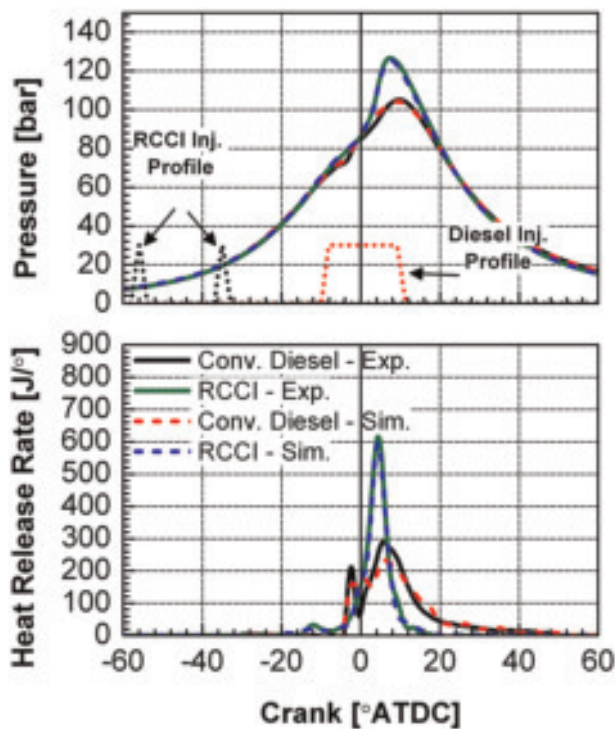
**Fig. 9** Measured and predicted cylinder pressure and AHRRs apparent heat release rates for conventional diesel and RCCI combustion at 9 bar IMEP

suggested as an upper limit by Dec and Yang. [11]. Additionally, model results show that, at this condition, nearly all of the UHC emissions result from the relatively large ring-pack crevice volume. Although beyond the scope of this work, it may be possible to reduce UHC and CO emissions through improvements in the ring-pack design.

Similar to the previous section, the simulation results are used to gain insight into the experimentally observed improvements of RCCI compared to conventional diesel operation. The improvements in $NO_x$ and soot are explained by plotting the simulation results in temperature–equivalence ratio space. Figure 10 shows the corresponding temperature and equivalence ratio for each computational

cell at 5° ATDC for the RCCI and conventional diesel combustion cases. It can be seen that, as expected, conventional diesel combustion has significant locally rich regions as well as lean high-temperature regions, which form soot and $NO_x$, respectively. The RCCI case shows that the peak equivalence ratio is near 0.6 and due to the combination of relatively lean operation and reduced intake oxygen concentration, the flame temperatures remain below the $NO_x$ formation threshold.

To understand the improvement in gross indicated efficiency, Fig. 11 shows the model-predicted HT losses. It can be seen that the RCCI case has 43 per cent lower HT losses than the conventional diesel case (i.e. 8.2 per cent less of the fuel energy is lost to HT).

Figure 12 shows the model-predicted average and peak temperatures for the RCCI and conventional diesel combustion events. It can be seen that the average temperatures are very similar; however, the peak combustion temperature for the conventional diesel case is near 2800 K; whereas the RCCI case shows a peak temperature near 1700 K. It should also be noted that the conventional diesel case has slightly higher average temperatures due to the slightly higher load operation as indicated in Table 7. When the exhaust energies are compared, it can be seen that the conventional diesel and RCCI cases result in nearly identical energy levels available to drive the turbocharger. Furthermore, Fig. 13 shows contours of the temperature predicted by the CFD modelling. It can be seen that not only does conventional diesel combustion have regions of the combustion chamber at significantly higher temperatures than the RCCI case, but these regions tend to be located on or near the piston bowl due to the penetration of the fuel jet. These high-temperature regions result in significantly increased piston bowl HT and reduced thermal efficiency.

While a majority of the improvements of the gross indicated efficiency can be attributed to reductions in HT losses, the remaining improvement in gross indicated efficiency is due to

**Table 8** Emissions and performance of RCCI and conventional diesel combustion

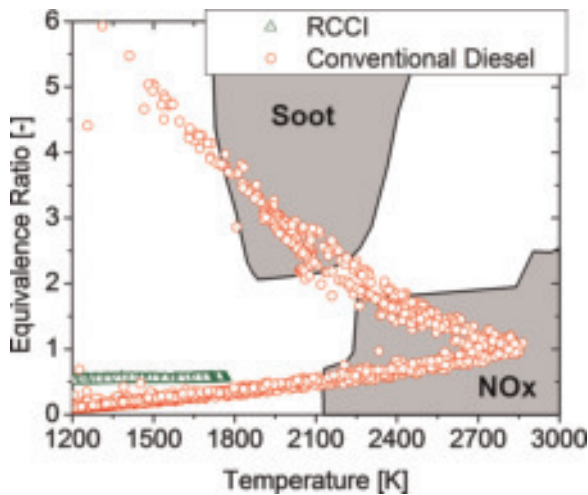|  | RCCI | | Conventional diesel | |
|---|---|---|---|---|
|  | Experiment | Simulation | Experiment | Simulation |
| $IS_{NOx}$ (g/kW-h) | 0.011 | 0.006 | 10 | 9.2 |
| $IS_{soot}$ (g/kW-h) | 0.012 | 0.019 | 0.076 | 0.133 |
| RI (MW/m$^2$) | 3.3 | 3.8 | 0.9 | 1 |
| Maximum PRR (bar/deg) | 9.7 | 10.3 | 4.9 | 5.2 |
| Gross indicated efficiency (%) | 56.1 | 54.3 | 48.2 | 47.6 |
| Combustion losses (%) | 2.0 | 1.3 | 0.1 | 0.3 |
| HT (%) | 11.4 | 10.9 | NA | 19.1 |
| Exhaust energy (%) | 30.5 | 33.4 | NA | 33.0 |

**Fig. 10** Equivalence ratio versus temperature plot comparing conventional diesel (circles) and RCCI combustion (triangles) at 5° ATDC. The $NO_x$ and soot islands are approximate and based on the work of Akihama *et al.* [45]



**Fig. 11** Model-predicted heat transfer losses for the conventional diesel (solid line) and RCCI (dashed line) cases of Table 7 normalized by the fuel energy

improved control over the combustion event. Recall that the RCCI combustion process converts ~8 per cent more of the fuel energy to useful work than the conventional diesel case. However, due to lower combustion temperatures and the fact that the engine was not designed to operate on a pre-mixed fuel – this engine has a large ring-pack crevice volume – the combustion efficiency is approximately 2 per cent lower for the RCCI combustion event. To make an accurate comparison of the energy release processes, care must be taken to evaluate the energy release without the influences of combustion efficiency. To make this comparison, the thermal efficiency, $\eta_{\text{thermal}}$, is defined as

$$\eta_{\text{thermal}} = \frac{W_g}{(\text{Fuel energy})\eta_{\text{comb.}}} \tag{4}$$

where $W_g$ is the gross indicated work and $\eta_{\text{comb.}}$ is the combustion efficiency. The thermal efficiency as defined by equation (4) of RCCI combustion is 9 per cent greater than that of conventional diesel.

The remaining improvements in thermal efficiency can be explained by improvements in the start- and end-of-combustion. Revisiting the pressure and heat release traces of Fig. 9 shows that, compared to the RCCI case, the conventional diesel combustion case has an earlier start-of-combustion and a later end-of-combustion (i.e. the combustion duration is longer). Each case shows combustion occurring slightly prior to TDC, which results in increased compression work, which cannot be fully recovered during the expansion stroke due to
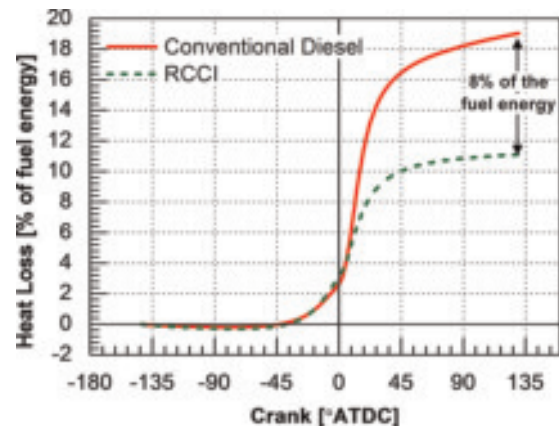
irreversibilities (e.g. HT). However, comparing the duration of combustion it can be seen that the rate of heat release falls off rapidly for the RCCI case and by 16° ATDC the combustion event has reached completion. In contrast to the RCCI case, the conventional diesel case continues to show slow energy release until nearly 40° ATDC. This late cycle burning results in reduced thermal efficiency due to the loss of expansion work.

To further the comparison and isolate the effects of only the combustion event, the simulations were used to evaluate adiabatic operation in both RCCI and conventional diesel combustion. Figure 14 shows the comparisons of cylinder pressure and AHRR for cases with and without HT. In the adiabatic cases, the IVC temperatures were adjusted slightly to provide the same combustion phasing as the cases considering HT. For the RCCI case the IVC temperature was reduced by 7 K and for the conventional diesel case the initial temperature was reduced by 5 K. Notice that, since the HT is eliminated, the peak AHRR for the RCCI case increases significantly. However, since the rate of heat release for conventional diesel combustion is controlled by transport (i.e. the transport of reactive material to the reaction zone) the combustion rate for the conventional diesel case is relatively insensitive to the elimination of HT. However, the RCCI case shows that aside from an increase in the peak heat release rate, the end of combustion is much more rapid. This is due to the elimination of cool regions near the cylinder liner where reaction rates are relatively low and combustion struggles to reach completion.

Table 9 shows the energy balances for each case. With adiabatic operation it can be seen that the gross indicated efficiency of each combustion mode increases by approximately 8 per cent of the fuel
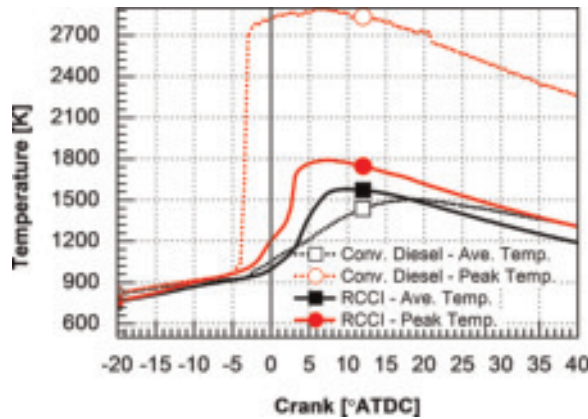
**Fig. 12** Comparison of model-predicted average (global) and peak (local) temperatures for RCCI and conventional diesel combustion
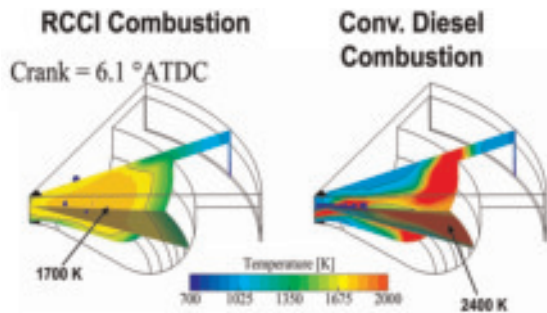


**Fig. 13** Temperature contours on cut-planes coincident with the spray axis at a 6.1° ATDC (i.e. near the 50 per cent burn location (CA50)) for RCCI and conventional diesel combustion



**Fig. 14** Cylinder pressure and heat release rate for cases with and without heat transfer for conventional diesel and RCCI combustion

energy. Further notice that the combustion efficiency of the RCCI case increases to nearly 100 per cent; however, the conventional diesel case shows very little increase in combustion efficiency. This is due to the fact that, in conventional diesel combustion, incomplete combustion occurs in two regions: overly lean regions outside of the spray plume and near the nozzle; and overly rich regions with insufficient oxygen in the centre of the plume. Since these combustion inefficiencies are primarily mixing-driven processes, they are relatively insensitive to the increased temperature resulting from the elimination of HT. However, in RCCI or any HCCI-type combustion (provided that the global equivalence ratio is above the lean oxidation limit: ~0.2 for operation without EGR), the primary causes of combustion inefficiency are unburned fuel located in low-temperature crevice regions and cool regions near the cylinder liner. In the adiabatic case, the entire chamber is compressed to the adiabatic core temperature and the fuel in the crevice regions is able to achieve complete combustion.
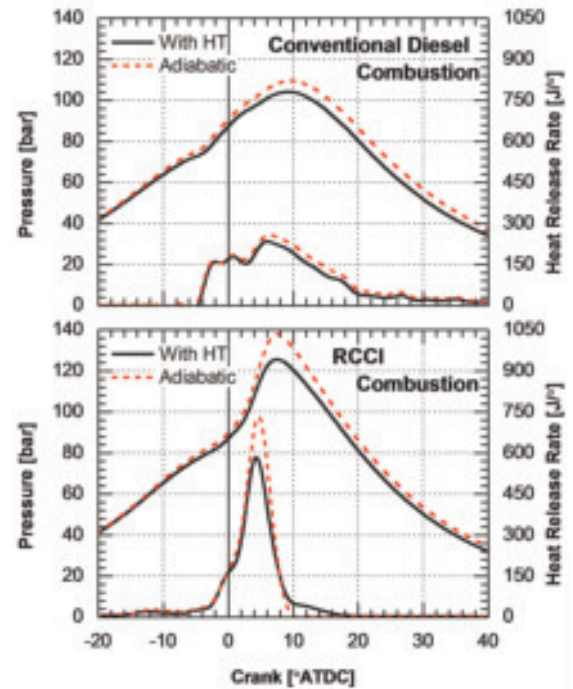
The primary purpose of this section was to evaluate the relative quantities of the removed heat loss that goes into work and exhaust energy. In order to make a direct comparison of the relative quantities of the removed HT losses that go to work and exhaust losses for the adiabatic cases, an assumption must be made regarding the combustion losses. To provide a conservative analysis, the increase in work due to increased combustion efficiency is removed from the analysis by subtracting the increased combustion efficiency from the gross indicated efficiency of Table 9 (i.e. $\eta_{\text{g.i., corrected}} = \eta_g - \eta_{\text{comb.}}$). With this assumption, the energy recovered by operating adiabatically must either go to increased work or exhaust energy. Figure 15 shows the partitioning of the HT energy to work and exhaust energy. It can be seen that the RCCI case converts 57.6 per cent of the recovered HT energy to useful work. Although the conventional diesel case shows a similar increase in gross indicated efficiency when adiabatic operation is considered, since the heat loss for the non-adiabatic conventional diesel case was significantly higher than for the non-adiabatic RCCI case, the relative percentage of the recovered heat loss that performs useful work is 14 per cent lower than for the RCCI case. Figure 15 clearly highlights the improved work extraction gained from improved control over the start- and end-of-combustion for the RCCI case.

**Table 9** Energy balance for RCCI and conventional diesel combustion with and without heat transfer

| | RCCI (simulation) | | Conventional diesel (simulation) | |
|---|---|---|---|---|
| | With HT | Adiabatic | With HT | Adiabatic |
| Gross indicated efficiency (%) | 54.3 | 61.9 | 47.6 | 56.0 |
| Combustion losses (%) | 1.3 | 0.0 | 0.3 | 0.3 |
| HT (%) | 10.9 | 0.0 | 19.1 | 0.0 |
| Exhaust energy (%) | 33.4 | 38.1 | 33.0 | 43.7 |
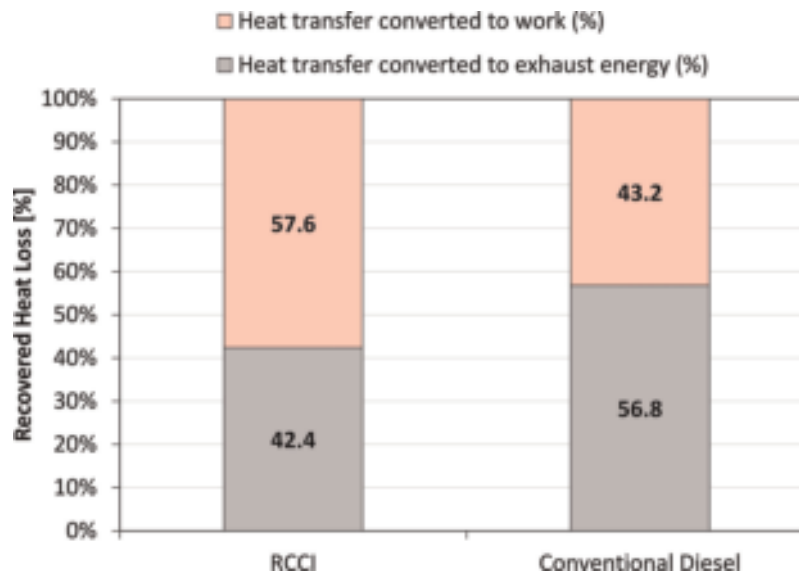


**Fig. 15** Partitioning of the recovered heat transfer from adiabatic operation energy to work and exhaust energy

Finally, to ensure the comparison of RCCI combustion and conventional diesel combustion was not biased due to differences in initial conditions, CFD modelling was used to compare RCCI combustion and conventional diesel combustion at the same operating conditions. The operating conditions for the modelling study are provided in Table 10. For the high-EGR diesel combustion case the injection timing was varied to achieve the same combustion phasing (CA50) as the RCCI case. Notice that the fuelling was held constant, thus the reduced efficiency of the high-EGR diesel case results in a lower IMEP. Table 11 shows the comparison of the computed emissions and performance. As expected, the reduced oxygen concentration of the high-EGR diesel combustion case results in significantly lower $NO_x$ emissions than the zero EGR conventional diesel case presented in the previous section (i.e. the results of Table 8). However, it can also be seen that the RCCI combustion case shows two orders of magnitude lower $NO_x$ emissions than high-EGR diesel combustion case. Recall that the high-EGR diesel and RCCI

cases have identical initial conditions; thus for a given equivalence ratio the global adiabatic flame temperatures would be identical. However, since the RCCI injection strategy allows sufficient time for mixing prior to reaction, the peak local equivalence ratio during the combustion process is only 0.6. The lean operation results in a peak temperature near 1700 K (see Fig. 10). Conversely, the high-EGR diesel case features a mixing-controlled combustion process where reactions occur in a near-stoichiometric band on the outer edge of the spray plume. Because combustion occurs in a stoichiometric region the peak temperature of the high-EGR diesel case is over 2500 K. From this comparison, it can be seen that the $NO_x$ reduction is due to the elimination of high temperature, near-stoichiometric regions. Of course it would be possible to reduce the flame temperatures of the high-EGR diesel case to 1700 K by further reducing the inlet oxygen concentration (i.e. increasing the EGR rate). Since it is expected that combustion would occur in a stoichiometric region for this case, the required level of EGR can be computed using

**Table 10** Operating conditions for the comparison between high-EGR diesel and RCCI combustion

|  | RCCI | High-EGR diesel |
|---|---|---|
| IMEP gross (bar) | 9.3 | 8 |
| Engine speed (rev/min) | 1300 | 1300 |
| Fuel flowrate (g/s) | 1.02 | 1.02 |
| Per cent gasoline (% by mass) | 89 | 0 |
| Air flowrate (kg/s) | 0.03 | 0,03 |
| DI SOI 1 (°ATDC) | −58 | −14 |
| DI SOI 2 (°ATDC) | −37 | NA |
| DI duration 1 (CA°) | 3.9 | 21 |
| DI duration 2 (CA°) | 1.95 | NA |
| Per cent of DI fuel in pulse 1 (% by mass) | 67 | 100 |
| DI injection pressure (bar) | 800 | 800 |
| Intake surge tank pressure (bar) | 1.74 | 1.74 |
| Exhaust surge tank pressure (bar) | 1.84 | 1.84 |
| Intake surge tank temperature (°C) | 32 | 32 |
| Air : fuel ratio (−) | 29 | 29 |
| EGR rate (%) | 41 | 41 |
| Fuel MEP (bar) | 16.6 | 16.6 |
| IVC (°ATDC) | −143 | −14.3 |
| EVO (°ATDC) | 130 | 130 |

**Table 11** Emissions and performance of RCCI and high-EGR diesel combustion

|  | RCCI | High-EGR diesel |
|---|---|---|
| ISno$x$ (g/kW-h) | 0.006 | 0.81 |
| ISsoot (g/kW-h) | 0.019 | 0.23 |
| RI (MW/m$^2$) | 3.8 | 1.4 |
| Max PRR (bar/deg) | 10.3 | 6.1 |
| Gross indicated efficiency (%) | 54.3 | 48.7 |
| Combustion losses (%) | 1.3 | 0.7 |
| HT (%) | 10.9 | 16.1 |
| Exhaust energy (%) | 33.4 | 34.5 |

homogenous reactor simulations. Assuming constant pressure combustion it is found that the inlet oxygen concentration must be reduced to 8.5 per cent by volume to achieve a stoichiometric flame temperature of 1700 K. To realize this reduction in inlet oxygen concentration at the present operating condition, the EGR must be increased to approximately 70 per cent.

In addition to a significant $NO_x$ reduction, the RCCI case shows ten times lower soot emissions. Finally, comparing the energy balances of Table 11, it can be seen that the RCCI combustion case results in an improvement in gross indicated efficiency of 11.5 per cent (i.e. the RCCI combustion case converts 5.6 per cent more of the fuel energy into useful work). Similar to the comparisons with conventional (zero EGR) diesel combustion, it appears that the improvement in gross indicated efficiency is primarily due to reduced HT losses.

## 7 CONCLUSIONS

This work further demonstrates the feasibility of a dual fuel RCCI concept that uses two fuels with different reactivities [**41**]. The present study used PFI of commercially available gasoline and DI of commercially available diesel fuel. The RCCI concept has been shown to provide improved control over the combustion process and to allow high-efficiency and low emissions operation over a wide range of speeds and loads. In the present work RCCI is demonstrated in a HD diesel engine

operating at 1300 rev/min with loads from 4.6 to 14.6 bar IMEP. Additional experimental results are available in the literature [**5**, **6**, **27**, **28**, **42**, **43**] over wider operating ranges and with different fuels.

The present study demonstrates that RCCI is a promising strategy to meet current and future emissions regulations without relying on $NO_x$ and soot after-treatment. Aside from the ability to meet $NO_x$ and soot emissions in-cylinder, RCCI is shown to provide high efficiency over a wide range of engine loads, with a peak gross indicated efficiency of 56 per cent at the 9.3 bar IMEP operating point.

To help understand the origins of the improved performance, engine experiments were used to compare RCCI and conventional diesel combustion. Compared to conventional diesel combustion without EGR it was found that RCCI results in a $NO_x$ reduction of nearly three orders of magnitude, six times lower soot, and 16.4 per cent higher gross indicated efficiency. In addition to the experimental engine comparisons, CFD modelling was used to compare RCCI and high-EGR diesel combustion. It was found that at identical operating conditions (e.g. equal inlet oxygen concentrations) $NO_x$ was reduced by two orders of magnitude, soot was reduced by a factor of ten, and gross indicated efficiency was improved by 11.5 per cent.

The CFD modelling indicates that the observed $NO_x$ and soot reductions are due to the avoidance of high equivalence ratio and high temperature regions in the combustion chamber. Two factors were found to explain the improved thermal efficiency. First, RCCI combustion avoids high-temperature regions that are located near the piston bowl surface that are observed in the conventional diesel combustion case; thus, HT losses are reduced by nearly a factor of two. Second, RCCI combustion shows improved control over the start- and end-of-combustion. This improved combustion control allows the combustion timing and duration to be optimized for minimum compression work and maximum expansion work (i.e. maximum

indicated efficiency). The improved control over the start- and end-of-combustion was highlighted by exploring adiabatic operation with the CFD modelling. It was found that when HT is removed the RCCI combustion process converts 14 per cent more of the recovered HT energy into useful work than conventional diesel operation.

## ACKNOWLEDGEMENTS

## REFERENCES

**1 Kim, J., Park, S. W.,** and **Reitz, R. D.** Improvements in the performance and pollutant emissions for stoichiometric diesel combustion engines using a two-spray-angle nozzle. *J. Automob. Engng*, 2010, **224**(8), 1113–1122.

**2 Theis, J. R., Ura, J. A., Li, J. J., Surnilla, G. G., Roth, J. M.,** and **Goralski Jr, C. T.** NOx release characteristics of lean NOx traps during rich purges. SAE paper 2003-01-1159, 2003.

**3 Turns, S. R.** *An introduction to combustion: concepts and applications*, second edition, 1999 (WCB/McGraw-Hill, Boston, Massachusetts).

**4 Manente, V., Tunestal, P.,** and **Johansson, B.** Partially premixed combustion at high load using gasoline and ethanol, a comparison with diesel. SAE paper 2009-01-0944, 2009.

**5 Splitter, D. A., Hanson, R. M., Kokjohn, S. L.,** and **Reitz, R. D.** Improving engine performance by optimizing fuel reactivity with a dual fuel PCCI strategy. Conference on Thermo and Fluid Dynamic Processes in Diesel Engines, Valencia, Spain, 14–17 September 2010.

**6 Kokjohn, S. L., Splitter, D. A., Hanson, R. M.,** and **Reitz, R. D.** Experiments and modeling of dual fuel HCCI and PCCI combustion using in-cylinder fuel blending. *SAE Int. J. Engines*, 2010, **2**(2), 24–39.

**7 Manente, V., Johansson, B., Tunestal, P.,** and **Cannella, W.** Effects of ethanol and different type of gasoline fuels on partially premixed combustion from low to high load. SAE paper 2010-01-0871, 2010.

**8 Hasegawa, R.** and **Yanagihara, H.** HCCI combustion in DI diesel engine. SAE paper 2003-01-0745, 2003.

**9 Hardy, W. L.** and **Reitz, R. D.** A study of the effects of high EGR, high equivalence ratio, and mixing time on emissions levels in a heavy-duty diesel engine for PCCI combustion. SAE paper 2006-01-0026, 2006.

**10 Opat, R., Ra, Y., Gonzalez, M. A., Krieger, R., Reitz, R. D., Foster, D. E., Siewert, R.,** and **Durrett, R.** Investigation of mixing and temperature effects on HC/CO emissions for highly dilute low temperature combustion in a light duty diesel engine. SAE paper 2007-01-0193, 2007.

**11 Dec, J. E.** and **Yang, Y.** Boosted HCCI for high power without engine knock and with ultra-low NOx emissions using conventional gasoline. *SAE Int. J. Engines*, 2010, **3**(1), 750–767.

**12 Manente, V., Johansson, B., Tunestal, P.,** and **Cannella, W.** Influence of inlet pressure, EGR, combustion phasing, speed and pilot ratio on high load gasoline partially premixed combustion. SAE paper 2010-01-1471, 2010.

**13 Kalghatgi, G. T.** Auto-ignition quality of practical fuels and implications for fuel requirements of future SI and HCCI engines. SAE paper 2005-01-0239, 2005.

**14 Kalghatgi, G., Risberg, P.,** and **Angstrom, H.** Advantages of fuels with high resistance to auto-ignition in late-injection, low-temperature, compression ignition combustion. *SAE Trans.*, 2006, **115**(4), 623–634.

**15 Kalghatgi, G. T., Risberg, P.,** and **Ångström, H.** Partially pre-mixed auto-ignition of gasoline to attain low smoke and low NOx at high load in a compression ignition engine and comparison with a diesel fuel. SAE paper 2007-01-0006, 2007.

**16 Liu, H., Yao, M., Zhang, B.,** and **Zheng, Z.** Effects of inlet pressure and octane numbers on combustion and emissions of a homogeneous charge compression ignition (HCCI) engine. *Energy and Fuels*, 2008, **22**(4), 2207–2215.

**17 Christensen, M., Hultqvist, A.,** and **Johansson, B.** Demonstrating the multi-fuel capability of a homogeneous charge compression ignition engine with variable compression ratio. SAE paper 1999-01-3679, 1999.

**18 Bessonette, P. W., Schleyer, C. H., Duffy, K. P., Hardy, W. L.,** and **Liechty, M. P.** Effects of fuel property changes on heavy-duty HCCI combustion. SAE paper 2007-01-0191, 2007.

**19 Inagaki, K., Fuyuto, T., Nishikawa, K., Nakakita, K.,** and **Sakata, I.** Dual-fuel PCI combustion controlled by in-cylinder stratification of ignitability. SAE paper 2006-01-0028, 2006.

**20 Ra, Y.** and **Reitz, R. D.** A reduced chemical kinetic model for IC engine combustion simulations with primary reference fuels. *Combust. Flame*, 2008, **155**(4), 713–738.

**21 Amsden, A. A.** KIVA-3V, Release 2, improvements to KIVA-3V, LA-UR-99-915, Los Alamos National Laboratory, 1999.

**22 Beale, J. C.** and **Reitz, R. D.** Modeling spray atomization with the Kelvin–Helmholtz/Rayleigh–Taylor hybrid model. *Atomiz. Sprays*, 1999, **9**(6), 623–650.

**23 Abani, N., Munnannur, A.,** and **Reitz, R. D.** Reduction of numerical parameter dependencies in diesel spray models. *Trans. ASME, J. Engng Gas Turbines Power*, 2008, **130**(3) 1–9.

**24 Abani, N., Kokjohn, S. L., Park, S. W., Bergin, M., Munnannur, A., Ning, W., Sun, Y.,** and **Reitz, R. D.** An improved spray model for reducing numerical parameters dependencies in diesel engine CFD simulations. SAE paper 2008-01-0970, 2008.

25 **Kong, S.-C., Sun, Y.,** and **Reitz, R. D.** Modeling diesel spray flame lift-off, sooting tendency and NOx emissions using detailed chemistry with a phenomenological soot model. *Trans. ASME, J. Engng Gas Turbines Power*, 2007, **129**, 245–251.

26 **Ra, Y.** and **Reitz, R. D.** The application of a multi-component droplet vaporization model to gasoline direct injection engines. *Int. J. Engine Res.*, 2003, **4**(3), 193–218.

27 **Hanson, R. M., Kokjohn, S. L., Splitter, D. A.,** and **Reitz, R. D.** An experimental investigation of fuel reactivity controlled PCCI combustion in a heavy-duty engine. SAE paper 2010-01-0864, 2010.

28 **Splitter, D. A., Hanson, R. M., Kokjohn, S. L., Rein, K., Sanders, S.,** and **Reitz, R. D.** An optical investigation of ignition processes in fuel reactivity controlled PCCI combustion. SAE paper 2010-01-0345, 2010.

29 **Shuai, S., Abani, N., Park, S. W., Yoshikawa, T.,** and **Reitz, R. D.** Simulating low temperature diesel combustion with improved spray models. *Int. J. Therm. Sci.*, 2009, **48**(9), 1786–1799.

30 **Hiroyasu, H.** and **Kadota, T.** Models for combustion and formation of nitric oxide and soot in DI diesel engines. SAE paper 760129, 1976.

31 **Sun, Y.** *Diesel combustion optimization and emissions reduction using adaptive injection strategies (AIS) with improved numerical models.* PhD Thesis, Department of Mechanical Engineering, University of Wisconsin-Madison, 2007.

32 **Munnannur, A.** *Droplet collision modeling in multi-dimensional engine spray computations.* PhD Thesis, Department of Mechanical Engineering, University of Wisconsin-Madison, 2007.

33 **O'Rourke, P. J.** and **Amsden, A. A.** A spray/wall interaction submodel for the KIVA-3 wall film model. SAE paper 2000-01-0271, 2000.

34 **O'Rourke, P. J.** and **Amsden, A. A.** A particle numerical model for wall dynamics in port-injected engines. SAE paper 961961, 1996.

35 **Kokjohn, S. L.** and **Reitz, R. D.** Investigation of the roles of flame propagation, turbulent mixing, and volumetric heat release in conventional and low temperature diesel combustion. *Trans. ASME, J. Engng Gas Turbines Power*, (accepted).

36 **Kokjohn, S. L.** and **Reitz, R. D.** A modeling study of charge preparation in an HCCI engine using a variable pressure pulse (VPP) injection system and optimized PRF Blends. The 11th International Conference on Liquid Atomization and Spray Systems, Vail, Colorado, 30 July 2009.

37 **Eng, J.** Characterization of pressure waves in HCCI combustion. SAE paper 2002-01-2859, 2002.

38 **McBride, B.** and **Gordon, S.** Computer program for calculation of complex chemical equilibrium compositions, rocket performance, incident and reflected shocks, and Chapman–Jouguet detonations, NASA report SP-273, National Air and Space Administration, 1971.

39 **Tess, M.** and **Reitz, R. D.** Diesel engine combustion size scaling at medium load without EGR. SAE paper 11PFL-1022, 2011.

40 **Ferguson, C. R.** and **Kirkpatrick, A. T.** *Internal combustion engines*, second edition, 2001 (John Wiley & Sons, New York, New York).

41 **Reitz, R. D., Hanson, R. M., Splitter, D. A.,** and **Kokjohn, S. L.** *Engine combustion control via fuel reactivity stratification.* University of Wisconsin WARF Patent Application P100054US.

42 **Hanson, R. M., Kokjohn, S. L., Splitter, D. A.,** and **Reitz, R. D.** Low load investigation of reactivity controlled compression ignition (RCCI) combustion in a heavy-duty engine. SAE paper 2011-01-0361.

43 **Splitter, D. A., Hanson, R. M., Kokjohn, S. L.,** and **Reitz, R. D.** Reactivity controlled compression ignition (RCCI) engine operation at mid and high loads with conventional and alternative fuels. SAE paper 2011-01-0363.

44 **Lutz, A. E., Kee, R. J.,** and **Miller, J. A.** SENKIN: A FORTRAN program for predicting homogeneous gas phase chemical kinetics with sensitivity analysis, SAND 89-8009, 1988.

45 **Akihama, K., Takatori, Y., Inagaki, K., Sasaki, S.,** and **Dean, A. M.** Mechanism of the smokeless rich diesel combustion by reducing temperature. SAE paper 2001-, 2001. paper number

## APPENDIX

### Definition of acronyms

| | |
|---|---|
| ATDC | after top dead centre |
| AHRR | apparent heat release rate |
| BDC | bottom dead centre |
| BTDC | before top dead centre |
| BMEP | brake mean effective pressure |
| CI | compression ignition |
| CFD | computational fluid dynamics |
| CA | crank angle |
| DPF | diesel particulate filter |
| DI | direct injection |
| ERC | engine research center |
| EPA | Environmental Protection Agency |
| EGR | exhaust gas recirculation |
| EVC | exhaust valve closing |
| EVO | exhaust valve opening |
| FSN | filter smoke number |
| HT | heat transfer |
| HD | heavy duty |
| HCCI | homogeneous charge compression ignition |
| IMEP | indicated mean effective pressure |
| IS | indicated specific |
| IVC | intake valve closure |

| | | | |
|---|---|---|---|
| IVO | intake valve opening | PRF | primary reference fuel |
| KH | Kelvin–Helmholtz | PID | proportional integral derivative |
| LDEF | Lagrangian-drop and Eulerian fluid | RT | Rayleigh–Taylor |
| | | RCCI | reactivity controlled compression ignition |
| LNT | lean $NO_x$ trap | RI | ringing intensity |
| LTC | low temperature combustion | SCR | selective catalytic reduction |
| LHV | lower heating value | SCOTE | single cylinder oil test engine |
| MEP | mean effective pressure | SI | spark ignited |
| PFI | port fuel-injection | SOI | start of injection |
| PCCI | premixed charge compression ignition | TWC | three-way catalyst |
| | | TDC | top dead centre |
| PCI | premixed compression ignition | UHC | unburned hydrocarbon |
| PM | particulate matter | US | United States |
| PRR | pressure rise rate | | |